applied sciences

MDPI

Article

Dependence of Dispersion on Metamaterial Structural Parameters and Dispersion Management

Zheng Guo Xu [1], Yan Ling Xue [1,2,*] and Zhihao Huang [1]

[1] Department of Communications Engineering, School of Information Science and Technology, East China Normal University, Shanghai 200241, China; xuzg2017@163.com (Z.G.X.); 18621933836@163.com (Z.H.)
[2] Collaborative Innovation Center of Extreme Optics, Shanxi University, Taiyuan 030006, Shanxi, China
* Correspondence: ylxue@ee.ecnu.edu.cn; Tel.: +86-21-6223-3253

Received: 12 April 2018; Accepted: 22 June 2018; Published: 28 June 2018

Featured Application: Although this is a theoretical work, it studies the dispersion characteristics in metamaterials in depth and discovers many results with potential applications in optical transmission.

Abstract: This paper compares the dispersion in metamaterials (MMs) and some Thorlabs' conventional glass, and finds that MMs may exhibit much more substantial dispersion (e.g., three orders of magnitude larger dispersion). With such large dispersion, a transmission more than 22 km is impossible because of pulse splitting resulting from the third-order dispersion. However, MMs are artificial materials with their electric and magnetic plasma frequencies tunable depending upon their structures. We take advantage of such tunability to tailor the dispersive response of MMs and investigate the dependence of dispersion on the MM structural parameters. We make dispersion management by (1) searching for the existence of some 'good' dispersion points and numerically demonstrating 90 km long transmission with almost no pulse width expansion and any impact from a higher order dispersion in the MM we designed; and (2) searching for the possibility for group-velocity dispersion (GVD) compensation and demonstrating 120 km transmission by configuring the dispersion-engineered MM.

Keywords: metamaterial; dispersion; nonlinear Schrödinger equation; Gaussian pulse; dispersion compensation

1. Introduction

Chromatic dispersion is the phenomenon in which the phase velocity of an optical wave depends on its frequency because of the material and structure's geometry [1]. Metamaterials (MMs) are materials engineered to have designed properties beyond those available in nature, with applications in all aspects of materials science [2,3]. In particular, MMs have shown promise for next generation optical materials with electromagnetic responses that cannot be obtained from conventional media. MMs are made from assemblies of multiple elements fashioned from composite materials, such as metals, plastics, or dielectric media. The materials are usually arranged in repeating patterns, at scales that are smaller than the wavelengths of the phenomena they influence. The regularly stacked structures in MMs may entail stronger chromatic dispersion. This paper makes a quantitative comparison of MMs to some conventional Thorlabs' glass [4,5], and discloses that MMs may have dispersion surpassing those of glass by three orders of magnitude. Since dispersion is a serious factor in MMs, dispersion management is an indispensable element while light propagates in MM waveguides, in which dispersive effects accumulate to set limits on both the distance and the bit rate of the data transfer.

Recent advances in nanofabrication and breakthroughs in the field of MMs [6–12] have opened up a new range of possibilities for obtaining optical properties on demand in MMs [13]. There is a research group now demonstrating that the group-velocity dispersion can be compensated by designing the phase-engineered MM, thus developing a new dispersion compensation technology [14]. The dispersive properties of most MMs are determined by the electric and magnetic plasma frequencies through the Drude model [15–17]. MMs are artificial materials with their electric and magnetic plasma frequencies tunable, depending upon their constituents and structures. Reconfigurable MMs provide flexibility for tuning them and result in tailored dispersive properties for dispersion management purposes. This paper studies the dependence of dispersion on the electric and magnetic plasma frequencies, and searches for the possibilities of dispersion management. Two approaches for the dispersion management are proposed. Demonstrations of a 90 km long transmission, with almost no pulse width expansion and any impact from a higher order dispersion in the MM we designed, and a 120 km transmission, by configuring the dispersion-engineered MMs, are numerically realized.

2. Theory of Light Pulse Propagations in MMs

Light is a type of electromagnetic wave and its propagation in MMs obeys Maxwell's equations. The wave equation for the light pulse propagating in nonlinear dispersive MMs can then be deduced as follows:

$$\frac{\partial^2 E}{\partial z^2} = \mu_0 \varepsilon_0 \frac{\partial^2 E}{\partial t^2} + \mu_0 \frac{\partial^2 P_{NL}}{\partial t^2}. \tag{1}$$

It is assumed that $E = 1/2A(z,t)\exp[i(\beta_0 z - \omega t)] + c.c$ and $P_{NL} = \varepsilon_0 \chi^{(3)} |E(z,t)|^2 E(z,t)$ with $\chi^{(3)}$ the third-order electric susceptibility. It is known that the relative dielectric constant ε_r and relative permittivity μ_r in a MM have to be dispersive, otherwise the energy density could be negative [15]. Their frequency dispersion can be described by a lossy Drude model [16–18], as follows:

$$\varepsilon_r = 1 - \frac{{\omega_{pe}}^2}{\omega(\omega + i\gamma_e)} \qquad \mu_r = 1 - \frac{{\omega_{pm}}^2}{\omega(\omega + i\gamma_m)}, \tag{2}$$

where ω is frequency, ω_{pe} and ω_{pm} are the respective electric and magnetic plasma frequencies. γ_e and γ_m are the respective electric and magnetic loss terms, which are very small. The loss appearing in the imaginary part of the Drude model has much of its effect on the light intensity only. In our model of dispersion compensation, the reduced intensity because of loss makes the waveform difficult for one to judge if the dispersion is fully compensated. Thereby, in the following analysis, we ignore loss for simplification. The negative refraction behavior is restricted within a certain range of frequency values. We can transform Equation (1) into the frequency space in order to expand $\varepsilon_r(\omega)$ and $\mu_r(\omega)$ in powers of ω, thus enabling us to treat the material parameters as a power series, which we can truncate to an appropriate order.

Taking the inverse Fourier transform, we also ignore the second derivative of z and introduce the group velocity reference frame $T = t - z/V_g \equiv t - \beta_1 z$. Then, we get the propagation equation for light pulse in MMs as follows:

$$\frac{\partial A}{\partial z} = -\frac{i}{2}\beta_2 \frac{\partial^2 A}{\partial T^2} + \frac{1}{6}\beta_3 \frac{\partial^3 A}{\partial T^3} - \frac{i}{24}\beta_4 \frac{\partial^4 A}{\partial T^4} + i\Gamma \left| A \right|_2 A. \tag{3}$$

The third-order nonlinear self-steepening effect that modulates the front edge and trailing edge of a Gaussian pulse in Equation (3) has been ignored, since what we study in the paper is the variation of the pulse shape due to higher order dispersion. However, the self-phase modulation effect remains. The third-order nonlinear self-phase modulation coefficient Γ and ith order dispersion β_i in Equation (3) can be expressed as follows:

$$\beta_i = \frac{d^i k}{d\omega^i}|_{\omega=\omega_0} \qquad (i = 1, 2, 3 \ldots\ldots), \tag{4}$$

$$\Gamma = \frac{\varepsilon_0 \mu_0 \chi^{(3)} \omega^2 \mu_r(\omega)}{2\beta_0}, \tag{5}$$

with k asthe wave number.

According to the definition of the index of refraction $n = \sqrt{\varepsilon_r \mu_r}$, we can deduce the ith order dispersion as follows [19]:

$$\beta_1 = \frac{dk}{d\omega} = \frac{1}{c}\left[n + \frac{1}{n}\left(\frac{1+\overline{\omega}_p{}^2}{\overline{\omega}^2} - \frac{2\overline{\omega}_p{}^2}{\overline{\omega}^4}\right)\right], \tag{6}$$

$$\beta_2 = \frac{d\beta_1}{d\omega} = \frac{1}{c\omega_{pe}}\left[\frac{1}{n\overline{\omega}}\left(-\frac{1}{\overline{\omega}^2} - \frac{\overline{\omega}_p{}^2}{\overline{\omega}^2} + 6\frac{\overline{\omega}_p{}^2}{\overline{\omega}^4}\right) - \frac{1}{n^3\overline{\omega}}\left(\frac{1+\overline{\omega}_p{}^2}{\overline{\omega}^2} - \frac{2\overline{\omega}_p{}^2}{\overline{\omega}^4}\right)^2\right], \tag{7}$$

$$\beta_3 = \frac{d\beta_2}{d\omega} = \frac{1}{c\omega_{pe}{}^2}\left\{\begin{array}{l} 3\left[\frac{1}{n}\left(-3\frac{1}{\overline{\omega}^4} - 3\frac{\overline{\omega}_p{}^2}{\overline{\omega}^4} + 10\frac{\overline{\omega}_p{}^2}{\overline{\omega}^6}\right) - \frac{1}{n^3}\left(\frac{1+\overline{\omega}_p{}^2}{\overline{\omega}^3} - \frac{2\overline{\omega}_p{}^2}{\overline{\omega}^5}\right)^2\right] \\ +\overline{\omega}\left[\begin{array}{l} \frac{1}{n}\frac{12\overline{\omega}_p{}^2\overline{\omega}^2 - 60\overline{\omega}_p{}^2 + 12\overline{\omega}^2}{\overline{\omega}^7} + \frac{3}{n^5}\left(\frac{\overline{\omega}_p{}^2\overline{\omega}^2 - 2\overline{\omega}_p{}^2 + \overline{\omega}^2}{\overline{\omega}^5}\right)^3 \\ +\frac{3}{n^3}\left(\frac{\overline{\omega}_p{}^2\overline{\omega}^2 - 2\overline{\omega}_p{}^2 + \overline{\omega}^2}{\overline{\omega}^5}\right)\left(\frac{3\overline{\omega}_p{}^2\overline{\omega}^2 - 10\overline{\omega}_p{}^2 + 3\overline{\omega}^2}{\overline{\omega}^6}\right) \end{array}\right] \end{array}\right\}, \tag{8}$$

$$\beta_4 = \frac{d\beta_3}{d\omega} = \frac{1}{c\omega_{pe}{}^3}\left\{\begin{array}{l} \frac{4\left(12\overline{\omega}_p{}^2\overline{\omega}^2 - 60\overline{\omega}_p{}^2 + 12\overline{\omega}^2\right)}{n\overline{\omega}^7} - \frac{3\left(3\overline{\omega}_p{}^2\overline{\omega}^2 - 10\overline{\omega}_p{}^2 + 3\overline{\omega}^2\right)}{n^3\overline{\omega}^{11}} \\ -\frac{60\overline{\omega}_p{}^2\overline{\omega}^2 - 420\overline{\omega}_p{}^2 + 60\overline{\omega}^2)}{n\overline{\omega}^7} - \frac{15\left(\overline{\omega}_p{}^2\overline{\omega}^2 - 2\overline{\omega}_p{}^2 + \overline{\omega}^2\right)^4}{n^7\overline{\omega}^{19}} \\ -\frac{4\left(\overline{\omega}_p{}^2\overline{\omega}^2 - 2\overline{\omega}_p{}^2 + \overline{\omega}^2\right)\left(12\overline{\omega}_p{}^2\overline{\omega}^2 - 60\overline{\omega}_p{}^2 + 12\overline{\omega}^2\right)}{n^3\overline{\omega}^{11}} \\ -\frac{9\left(\overline{\omega}_p{}^2\overline{\omega}^2 - 2\overline{\omega}_p{}^2 + \overline{\omega}^2\right)^2\left(6\overline{\omega}_p{}^2\overline{\omega}^2 - 20\overline{\omega}_p{}^2 + 6\overline{\omega}^2\right)}{n^5\overline{\omega}^{15}} \\ +\frac{12\left(\overline{\omega}_p{}^2\overline{\omega}^2 - 2\overline{\omega}_p{}^2 + \overline{\omega}^2\right)^3}{n^5\overline{\omega}^{15}} \\ +\frac{12\left(\overline{\omega}_p{}^2\overline{\omega}^2 - 2\overline{\omega}_p{}^2 + \overline{\omega}^2\right)\left(3\overline{\omega}_p{}^2\overline{\omega}^2 - 10\overline{\omega}_p{}^2 + 3\overline{\omega}^2\right)}{n^3\overline{\omega}^{11}} \end{array}\right\}, \tag{9}$$

where $\overline{\omega} = \frac{\omega}{\omega_{pe}}$ and $\overline{\omega}_p = \frac{\omega_{pm}}{\omega_{pe}}$ are the normalized light frequency and plasma frequency. The third-order nonlinear coefficient can also be simplified as follows:

$$\Gamma = \frac{\chi^{(3)}\overline{\omega}\omega_{pe}(1 - \frac{\overline{\omega}_p{}^2}{\overline{\omega}^2})}{2nc}. \tag{10}$$

3. Dispersion in a Regularly Exampled MM

We plot the refractive index, dispersion coefficients, and third-order nonlinear coefficient in Figure 1 based on Equations (6) and (7). Although the MM structural parameters ω_{pe} and ω_{pm} can be tuned, we employ the regularly exampled parameters with third-order electric susceptibility $\chi^{(3)}$ as 1.9×10^{-9} W^{-1} [20], ω_{pe} as 1.3673×10^{16} Hz [21], and $\overline{\omega}_p$ as 0.8 [22].

In Figure 1a, the normalized frequency can be divided into three domains, with $0 < \overline{\omega} < 0.8$ as the negative refractive index domain and $\overline{\omega} > 1.0$ as the positive refractive index domain, respectively. The intervening region $0.8 \leq \overline{\omega} \leq 1.0$ is the so called anomalous absorptive domain in the MM, in which the electromagnetic wave cannot propagate. It should be mentioned that (1) in Figure 1d β_2 increases from negative to positive in the negative refractive index region, with its zero point at $\overline{\omega}_D = 0.706844$; (2) in Figure 1e β_3 is always greater than zero in both the positive and negative refractive index regions, and becomes very smooth while it is far away from the anomalous absorptive domain; (3) in Figure 1f β_4 is always positive in the negative refractive index region.

Let's compare Figure 1 to the traditional media listed in Figure 2. Figure 2a,c, obtained from Thorlabs website [4,5], show the β_2 and β_3 of four conventional glass as a function of wavelength. In order to compare Figure 2a,c with Figure 1d,e, we need to unify the different units of abscissa in

these figures. We thereby obtain Figure 2b,d by redrawing Figure 2a,c with modified abscissa and ordinate units. From Figure 2b it can be seen that β_2 of these conventional glass are all very small, with the order of magnitude at only 10^{-1}. However, β_2 in Figure 1d is 10^4 nearby $\overline{\omega}_D$. It can be estimated if extending the β_2 curves in Figure 2b to $\overline{\omega}_D$, following the current trend, the absolute value $|\beta_2|$ should still be smaller than that in Figure 1d. Thus, we may say that $|\beta_2|$ of the MM, with the regularly used ω_{pe} and ω_{pm} is much larger than that in the conventional glass. Similarly, from Figure 2d, it can be seen that β_3 of these conventional glass are all very small, with the order of magnitude at only 10^{-4}. However, β_3 in Figure 1e is 10^0, nearby $\overline{\omega}_D$. It can be estimated that, if extending the β_3 curves in Figure 2d to $\overline{\omega}_D$, following the current trend, the absolute value $|\beta_3|$ should still be smaller than that in Figure 1e. Therefore, we may say that $|\beta_3|$ of the MM with the regularly used ω_{pe} and ω_{pm} is much stronger than that in the conventional glass. What is the impact of such high dispersions in the MM? We find out these effects by studying the light pulse propagation in the MM.

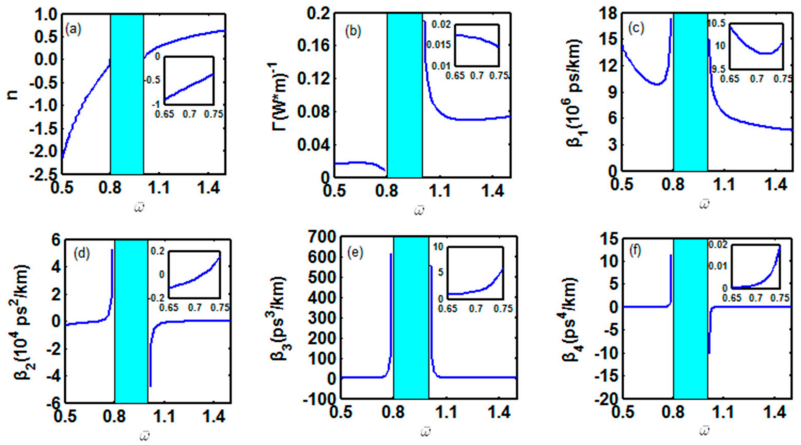

Figure 1. Variations of refractive index, third-order nonlinear coefficient, first-, second-, third-, and forth-order dispersion on $\overline{\omega}$. Insets are the magnification nearby $\overline{\omega} = 0.7$. (**a**) Refractive index versus $\overline{\omega}$; (**b**) third-order nonlinear coefficient versus $\overline{\omega}$; (**c**) first-order dispersion versus $\overline{\omega}$; (**d**) second-order dispersion versus $\overline{\omega}$; (**e**) third-order dispersion versus $\overline{\omega}$; and (**f**) forth-order dispersion versus $\overline{\omega}$.

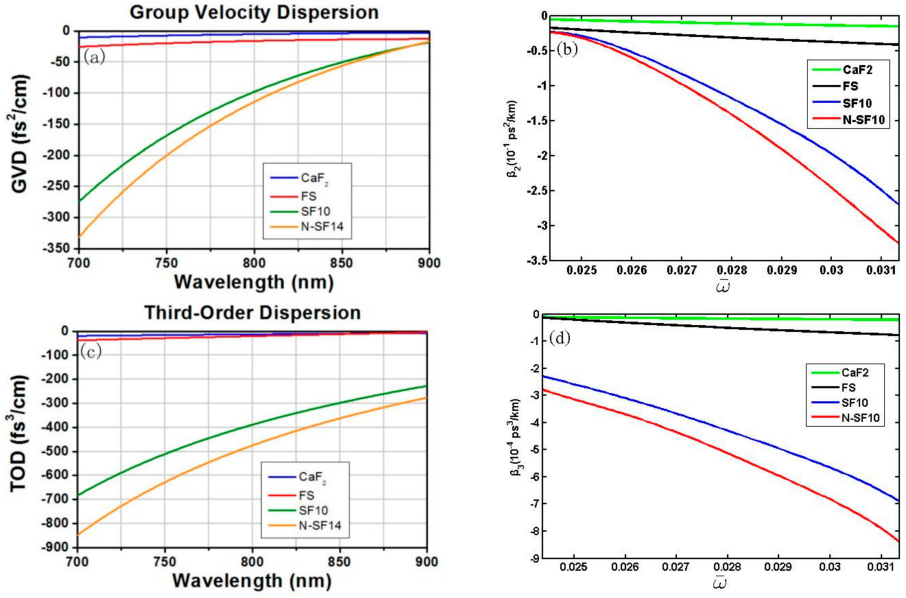

Figure 2. (**a**,**c**) Second- and third-order dispersions in several conventional glass verse wavelength; (**b**,**d**) redrawing (**a**,**c**) to the normalized frequency.

4. Light Pulse Propagation in the MM

The split-step Fourier method that has been used extensively to solve the pulse-propagation problem in nonlinear dispersive media is a kind of effective beam propagation methods (BPM) [19]. We employ the split-step Fourier method to simulate the propagation of the light pulse in the MM. The incident pulse is the Gaussian pulse with T_0, the half pulse width at the $1/e$ of the optical peak intensity. The full width at the half maximum (FWHM) is taken to be $T_{FWHM} = 5ps$ in the simulation, which is equivalent to a bit rate of 200 Gbps. The second- and third-order dispersion length are L_D and L'_D, respectively. The discussion of propagation issues requires the MM with a relatively long length. Although currently there is limitation in making long length MMs, we believe that in the near future, the technology will have breakthroughs in long length MM manufacture.

4.1. Impact of β_2 and β_3

4.1.1. Impact of β_2 at $\overline{\omega}_D$

The zero dispersion frequency $\overline{\omega}_D = 0.706844$ (with $\beta_2 = 0$) in Figure 1d means the Gaussian pulse can propagate in the MM forever with no pulse spreading due to β_2. This is a specific phenomenon in the MM and seems an ideal circumstance. From Figure 1e, there is $\beta_3 = 2.0698\ \mathrm{ps}^3/\mathrm{km}$ at $\overline{\omega}_D$. This β_3 is large so that the corresponding dispersion length is only $L'_D = 60.39$ km. To have a fair idea of when and how β_3 takes effect, we simulate the propagation of the Gaussian pulse in Figure 3.

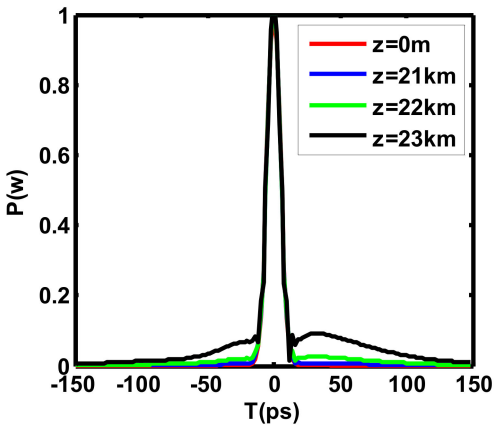

Figure 3. Pulse waveforms at different distances when $\beta_2 = 0$.

It is shown in Figure 3 that Gaussian pulse keeps its original waveform unchanged at $z < 21$ km. However, at around $z = 22$ km, the pulse starts forming a splitting peak under the influence of β_3. Although the pulse splitting just starts around $z = 22$ km, it develops quickly and has become obvious, while the pulse just transmits one more kilometer. This illustrates that β_3 starts to take its effect at a much earlier distance than $L'_D = 60.39$ km, and when a pulse transmits 60.39 km, the impact of β_3 should be very serious, so that the original pulse waveform may be completely ruined. We have pointed out in the former section that β_3 in the MM is four orders of magnitude stronger than that in ordinary glass. It is such a super larger third-order dispersion that pulse splitting starts at a short distance. Thus, although an ideal circumstance of $\beta_2 = 0$ predicts an infinite transmission, the strong β_3 limits the practical transmission to a very short distance. Therefore, we need to alter our perspective by seeking an occurrence with the compensated β_2 and very small β_3. In the following two sections, we first discuss the situation nearby the zero-dispersion frequency $\overline{\omega}_D$.

4.1.2. Impact of β_2 and β_3 when $\overline{\omega} < \overline{\omega}_D$

When $\overline{\omega} < \overline{\omega}_D$ in Figure 1d, there is $\beta_2 < 0$. Two sets of data are listed in Table 1 with different $|\beta_2|$ but little varied β_3. In addition, β_3 is chosen to be close to the data discussed in Section 4.1.1. Thus, L'_D is closed to that in the last section. Figure 4 shows the waveform plot corresponding to the two cases in Table 1. Similarly, the pulse starts to split around $z = 22$ km, although L'_D exceeds 60 km.

Table 1. Two sets of dispersion data for $\overline{\omega} < \overline{\omega}_D$.

$\overline{\omega}$	β_2 (ps^2/km)	β_3 (ps^3/km)	L_D (km)	L'_D (km)
0.70680	−1.2589	2.0676	19.86	60.46
0.70675	−2.6715	2.0675	9.36	60.53

In comparison to Figure 4a,b, we can see that for the second case in Table 1, where $|\beta_2|$ is relatively larger, the secondary peak generated from the pulse splitting is a little far from the main peak and its peak intensity is relatively smaller. Thus, it may say that, to some extent, a larger $|\beta_2|$ can inhibit the influence of pulse splitting. In addition, Figure 4 also show that the secondary peak appears at the front edge of the pulse if $\beta_2 < 0$. We also noted that the pulse splitting in Figure 4b is not so serious as that in Figure 3, although β_3 is similar. Again, this is due to the inhabitation of β_2 to the pulse splitting.

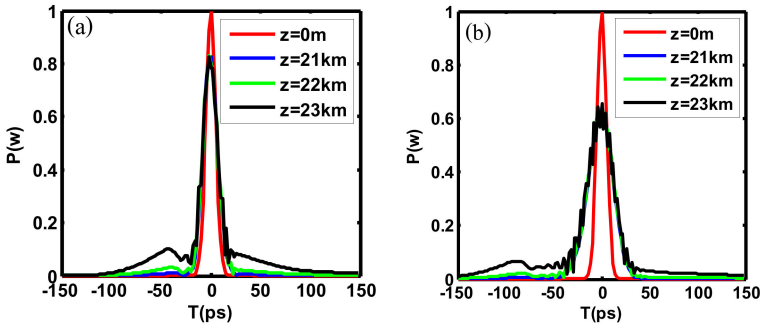

Figure 4. The pulse waveform comparison at different propagation distances. (**a**) The first case in Table 1; and (**b**) the second case in Table 1.

4.1.3. Impact of β_2 and β_3 when $\overline{\omega} > \overline{\omega}_D$

When $\overline{\omega} > \overline{\omega}_D$ in Figure 1d, there is $\beta_2 > 0$. Two sets of data are listed in Table 2, with different β_2 but little varied β_3. Similarly, β_3 is chosen to be close to the data discussed in Section 4.1.1. Figure 5 shows the waveform plot corresponding to Table 2. Similarly, the pulse starts to split around $z = 22$ km, although L'_D exceeds 60 km. The major difference between Tables 1 and 2 is the sign of β_2, but β_2 always causes pulse broadening, no matter its sign. So, Figure 5 is similar to Figure 4. The difference is that the secondary peak appears at the rear edge of the pulse if $\beta_2 > 0$. It also illustrates that, to some extent, a larger $|\beta_2|$ can inhibit the influence of the pulse splitting. We also noted that the pulse splitting in Figure 5d is not as serious as that in Figure 3, in spite of a higher β_3 here. Again, this is due to the inhabitation of β_2.

Table 2. Two sets of dispersion data for $\overline{\omega} > \overline{\omega}_D$.

$\overline{\omega}$	β_2 (ps^2/km)	fi$_3$ (ps^3/km)	L_D (km)	L'_D (km)
0.70690	1.5715	2.0726	15.91	60.31
0.70695	2.9894	2.0752	8.36	60.24

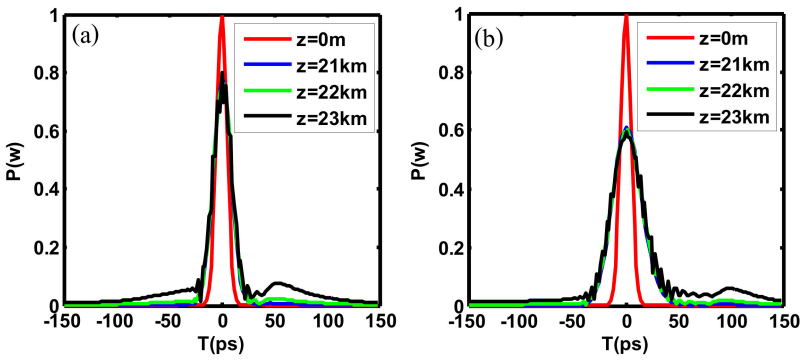

Figure 5. The pulse waveform comparison at different propagation distances. (**a**) The first case in Table 2; and (**b**) the second case in Table 2.

4.2. Impact of β_2, β_3, and β_4

In conventional media, the influence of β_4 can be ignored as it is so small. Section 3 shows that β_4 in the MM may be larger than that in the ordinary materials, however, it is just in 10^{-3} order of magnitude around $\overline{\omega}_D$, three orders of magnitude smaller than β_3 (Figure 1f). What is its impact?

There are two groups of data in Table 3, in which $|\beta_2|$, β_3, and β_4 are not much different, except for the different sign for β_2. In Figure 6, the red line represents the portion of the pulse waveform only under the impact of β_2 and β_3, while the blue one represents the similar waveform under the simultaneous impact of β_2, β_3, and β_4. It is shown from a comparison to the details after the magnification of the red and blue lines at $z = 21$ km that for $\beta_2 < 0$ in Figure 6a, the blue line is lower than the red line, representing a somewhat inhibition of β_2 to the pulse broadening, while for $\beta_2 > 0$ in Figure 6b, it is opposite, representing a little aggravation of β_2 to the pulse broadening. We also find that β_4 has no effect on the position of pulse splitting.

Table 3. Two sets of dispersion data including β_4.

$\overline{\omega}$	$\beta_2(\mathbf{ps^2/km})$	$\beta_3(\mathbf{ps^3/km})$	$\beta_4(\mathbf{ps^4/km})$	$L_D(\mathbf{km})$	$L'_D(km)$
0.706587	−7.2648	2.0569	0.0037	3.44	60.77
0.70710	7.2532	2.0828	0.0037	3.45	60.02

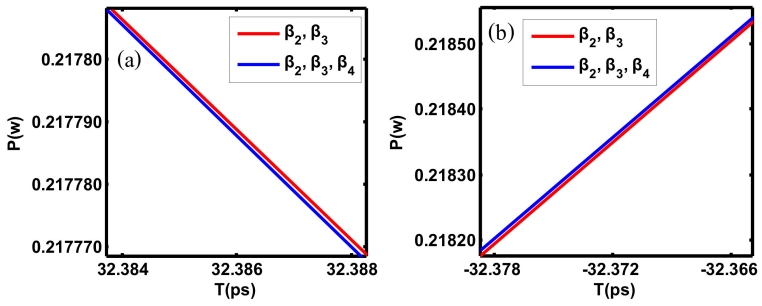

Figure 6. Magnification of the partial propagation waveform at FWHM for $z = 21$ km. (**a**) The first case in Table 3; and (**b**) the second case in Table 3.

5. Dispersion Management in MMs

5.1. Design of the Optimal Dispersion

From the above analyses, it is realized that the second- and third-order dispersions are all serious for that particular MM, which is often exampled in the literature with $\omega_{pe} = 1.3673 \times 10^{16}$Hz and

$\overline{\omega}_p = 0.8$ [21,22]. This makes the propagation with $z > 22$ km impossible. However, MMs are such extraordinary materials that derive their properties not only from the properties of the base materials, but from their newly artificially designed structures. Their precise shape, geometry, size, orientation, and arrangement give them their smart properties capable of manipulating electromagnetic waves to achieve benefits that go beyond what is possible with conventional materials. Therefore, we expand on our views to other MMs with different ω_{pe} and ω_{pm} (i.e., $\overline{\omega}_p$), and take insight into the dependence of dispersion to the structural parameters ω_{pe} and ω_{pm}. To obtain small second- and third-order dispersions for a reasonably long transmission, we present here the design of an MM by using the nano-inclusions model [23], made of properly arranged collections of plasmonic metallic nano-rings.

In our design, the nano-rings are made of a typical metal like aluminum, with its electrical plasma frequency described by $\omega_{pe} = \sqrt{Nq_e^2/(m\varepsilon_0)}$, where N is the density of electrons, q_e is the electron charge, m is the electron mass, and ε_0 is the dielectric permittivity in a vacuum [24]. For aluminum, the number of electrons per cubic meter can be $N = 1.806 \times 10^{29}\mathrm{m}^{-3}$ [16], then, there is $\omega_{pe} = 2.396 \times 10^{16}$Hz. When such aluminum nano-rings are embedded in a host medium, they may provide metamaterials with negative effective permeability at optical frequencies. According to the nano-inclusions model by the authors of [23], we calculated the effective permeability for the periodic arrangement of the aluminum nano-rings. The resonant magnetic dipole collective response of the effective permeability is presented in Figure 7, with R = 40 nm, a = 16 nm, N = 6, and N_d = (108 nm)$^{-3}$. Following [25,26], the damping frequency and high frequency dielectric constant of aluminum have been assumed to follow the Drude model with $\omega_\tau = 194$ THz and $\varepsilon_\infty = 1.65\varepsilon_0$. The background material in this design is $\varepsilon_b = 1.2\varepsilon_0$. With the effective magnetic permeability, the magnetic plasma frequency ω_{pm} can be obtained following the Drude model.

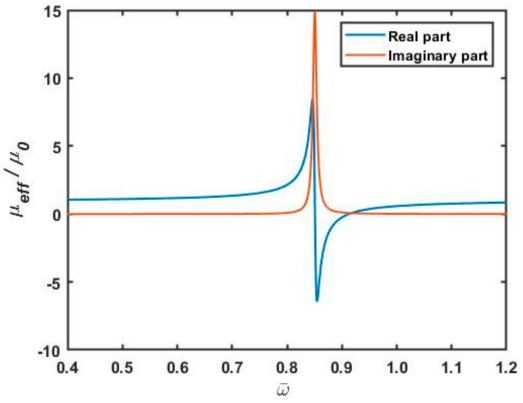

Figure 7. Effective relative magnetic permeability for bulk medium with the geometry of nano-rings.

Using Equation (6), we also obtained a group of 3D plots in Figure 8 for $0.1 \leq \overline{\omega} \leq 0.9$ and $0.1 \leq \overline{\omega}_p \leq 2$, with the fixed $\omega_{pe} = 2.396 \times 10^{16}$Hz. According to the definition, the range of $\overline{\omega}_p$ here, gives out the range of ω_{pm}. We search in Figure 8 for all of the values of ω_{pm} gained from our above design to check up their dispersion parameters, and hope to find the potential figures with lower dispersions. We pick out all points with approximately zero β_2 and very low β_3. Forty eight points with the second-order dispersion length $L_D > 525$ km and the third-order dispersion length $L'_D \approx 290$ km are found (see Appendix A). Among them, the best three points with the longest L'_D and an extremely low second-order dispersion are listed in Table 4. Figure 9 is an example of 90 km of a repeaterless transmission for the second group of data in Table 4. Within this distance, there is almost no expansion due to group-velocity dispersion (GVD) and any impact from third-order dispersion whose impact emerges while $z \geq 90$ km. Although we point out that the MM with $\omega_{pe} = 1.3673 \times 10^{16}$ Hz and $\overline{\omega}_p = 0.8$ [21,22] exhibits serious dispersion, it is delightful to see the MM we designed is not incurable

in dispersion and can be employed for long distance transmission in the future, when long-length MMs are ready.

Table 4. Examples for the lowest second- and third-order dispersions with $\omega_{pe} = 2.396 \times 10^{16}$Hz.

$\overline{\omega}$	$\overline{\omega}_p$	$\omega_{pm} \times 10^{16}(Hz)$	$\beta_2(\mathrm{ps^2/km})$	$\beta_3(\mathrm{ps^3/km})$	$\beta_4(\mathrm{ps^4/km})$	$L_D(\mathrm{km})$	$L'_D(\mathrm{km})$
0.8794313	1.277639	3.061222	0.002528	0.431002	0.0003325	9889.982	290.0218
0.8794314	1.277637	3.0612173	0.000674	0.431001	0.0003325	37111.35	290.0227
0.8794315	1.277635	3.0612125	−0.00118	0.430999	0.0003325	21177.19	290.0237

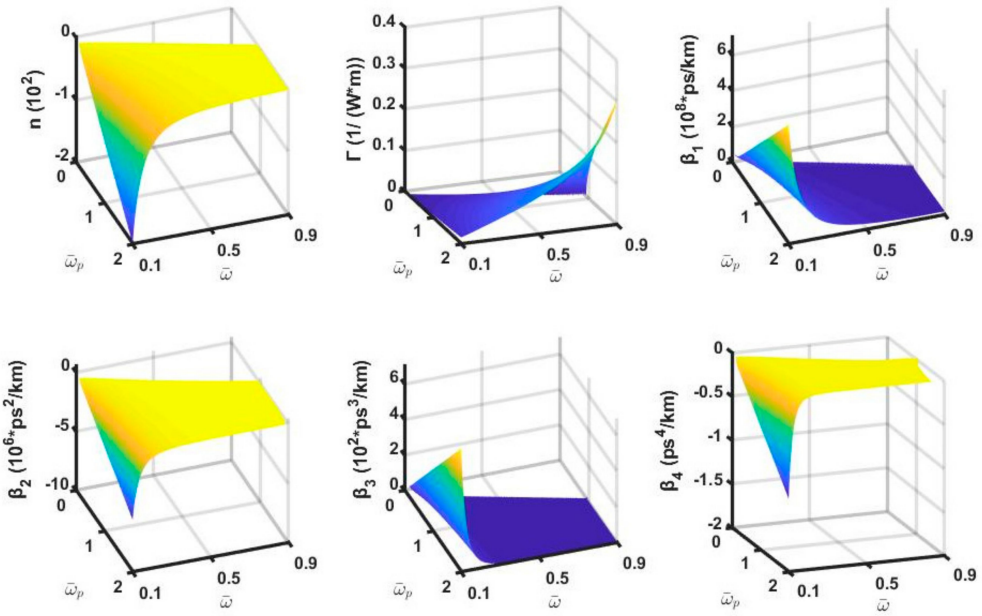

Figure 8. Dependence of refractive index, third-order nonlinear coefficient, first-, second-, third-, and forth-order dispersion on $\overline{\omega}$ and $\overline{\omega}_p$, with $\omega_{pe} = 2.396 \times 10^{16}$Hz.

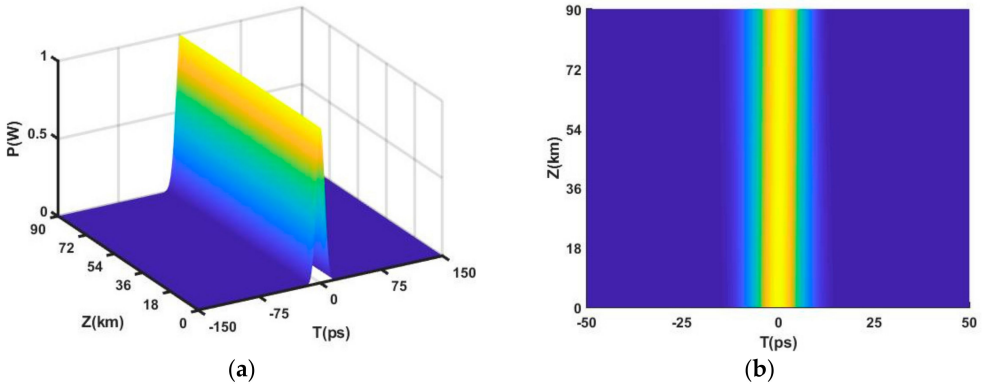

Figure 9. (**a**) Gaussian pulse's 90 km propagation; (**b**) top view of (**a**).

5.2. Dispersion Management

Dispersion compensation is for the circumstance in which β_2 and β_3 can both be compensated or β_2 is compensated, but β_3 is very small. According to the dispersion compensation theory, to reach the compensation for both β_2 and β_3, there should be the following [19]:

$$\beta_{21}L_1 + \beta_{22}L_2 = 0 \qquad \beta_{31}L_1 + \beta_{32}L_2 = 0 \tag{11}$$

where $L = L_1 + L_2$ is dispersion period, β_{2j} and β_{3j} (j = 1, 2) are second- and third-order dispersion for the MM with length L_j.

Figure 8d shows that β_2 can be positive and negative, so there is a possibility to reach β_2 compensation. However, in Figure 8e, β_3 is always positive, meaning that we cannot find a negative valued β_3 to reach its compensation. Luckily, for the same normalized frequencies we found two sets of data in Table 5 with an opposite notation and very closed absolute values of β_2 for compensation. Additionally, both sets of data all have very low β_3, resulting in L'_D as long as 380 km. That is to say, while the broadening due to the GVD is compensated, the effect due to the third-order dispersion has not yet emerged. Thus, we propose a configuration with metamaterials MM1 and MM2, cross-linked periodically with their length $L_1 = L_2 = 20$ km. The simulation results for the propagation of the Gaussian pulse in the composite metamaterial MM1 and MM2 is demonstrated in Figure 10.

Table 5. Two sets of data for β_2 compensation with $\omega_{pe} = 3.3673 \times 10^{16}$Hz.

Metamaterial	$\overline{\omega}$	$\overline{\omega}_p$	$\beta_2(\mathbf{ps^2/km})$	$\beta_3(\mathbf{ps^3/km})$	$L_D(\mathbf{km})$	$L'_D(\mathbf{km})$
MM1	0.88	0.941095	1.184911	0.330214	21.10	378.56
MM2	0.88	0.941240	−1.183498	0.327182	21.12	382.03

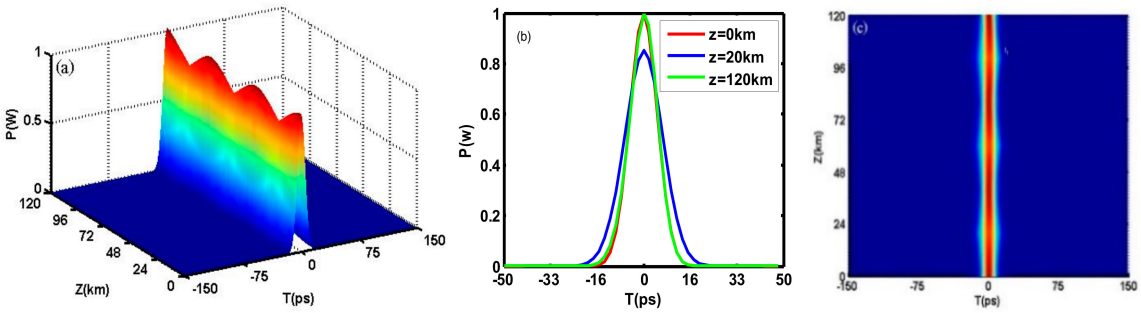

Figure 10. (**a**) Gaussian pulse's 120 km propagation in MM1 and MM2; (**b**) waveforms of the Gaussian pulse; (**c**) top view of (**a**).

Figure 10 shows that when the pulse transmits in MM1, its width spreads with the increase of the propagation distance, and the pulse intensity lowers because of the pulse broadening. At the propagation distance $L_1 = 20$ km, the pulse intensity reduces 20%. At this time, if we let the pulse enter into MM2 and it continually transmits inside MM2, the reduced intensity starts to be recovered and the broadened width gradually shrinks. At $Z = L_1 + L_2 = 20 + 20 = 40$ km, the intensity and the width have both been recovered to be equivalent to their initial values. The situation afterwards repeats the first MM1 and MM2 period, until it transmits $Z = 120$ km. While the pulse transmits one MM1 and MM2 period, the impact of β_3 remains uncompensated and accumulates with the increment of the transmission distance. The simulation shows that while the propagation distance approaches 140 km, the pulse splitting due to β_3 starts to emerge. Therefore, the MM1 and MM2 cross-linked structure allows a 120 km repeaterless transmission.

6. Conclusions

The paper studies the dispersion in MMs and finds that the GVD and higher order dispersion in MMs may often be much more serious than that in conventional glass. Since obtaining optical properties on demand by reconfiguring the MM constitutes and structure has not been unreachable, we may be able to design MMs and obtain the dispersive properties at extensive electric and magnetic plasma frequency ranges with desire. Thus, we investigate the relationship of dispersion with the MM structural parameters ω_{pe} and ω_{pm}, propose two approaches with the optimal dispersion

through the MM design and the composite metamaterial MM1 and MM2 for dispersion management, and demonstrate 90 km and 120 km long distance successful transmission, respectively.

Author Contributions: Y.L.X. conceived and designed the work; Z.G.X. and Z.H performed the numerical calculation; Y.L.X. and Z.G.X. analyzed the data; and Z.G.X. and Y.L.X. wrote the paper.

Funding: The National Key Research and Development Program of China (Grant No. 2016YFA0302000), and the National Natural Science Foundation of China (Grant No. 11234003).

Acknowledgments: This work was supported by the National Key Research and Development Program of China, under Grant No. 2016YFA0302000, and the National Natural Science Foundation of China, under Grant No. 11234003.

Conflicts of Interest: The authors declare no conflict of interest.

Appendix A

Table A1. All points in Figure 7 with $L_D \geq 525.93$ km and $L' \approx 290$ km.

$\overline{\omega}$	$\overline{\omega}_p$	$\omega_{pm} \times 10^{16}(Hz)$	$\beta_2(\mathbf{ps^2/km})$	$\beta_3(\mathbf{ps^3/km})$	$\beta_4(\mathbf{ps^4/km})$	$L_D(\mathbf{km})$	$L'_D(\mathbf{km})$
0.8794293	1.277678	3.061317	0.039611	0.431031	0.0003325	631.1424	290.0022
0.8794294	1.277676	3.0613123	0.037757	0.43103	0.0003325	662.1362	290.0032
0.8794295	1.277674	3.0613075	0.035902	0.431028	0.0003325	696.3313	290.0042
0.8794296	1.277672	3.0613028	0.034048	0.431027	0.0003325	734.2507	290.0051
0.8794297	1.27767	3.061298	0.032194	0.431025	0.0003325	776.5378	290.0061
0.8794298	1.277668	3.0612933	0.03034	0.431024	0.0003325	823.9935	290.0071
0.8794299	1.277666	3.0612885	0.028486	0.431023	0.0003325	877.6269	290.0081
0.87943	1.277664	3.0612838	0.026632	0.431021	0.0003325	938.7285	290.009
0.8794301	1.277662	3.061279	0.024778	0.43102	0.0003325	1008.975	290.01
0.8794302	1.27766	3.0612743	0.022923	0.431018	0.0003325	1090.585	290.011
0.8794303	1.277658	3.0612695	0.021069	0.431017	0.0003325	1186.558	290.012
0.8794304	1.277656	3.0612648	0.019215	0.431015	0.0003325	1301.054	290.013
0.8794305	1.277654	3.06126	0.017361	0.431014	0.0003325	1440.005	290.0139
0.8794306	1.277652	3.0612553	0.015507	0.431012	0.0003325	1612.186	290.0149
0.8794307	1.27765	3.0612505	0.013653	0.431011	0.0003325	1831.133	290.0159
0.8794308	1.277648	3.0612458	0.011799	0.431009	0.0003325	2118.896	290.0169
0.8794309	1.277647	3.061241	0.009944	0.431008	0.0003325	2513.967	290.0178
0.879431	1.277645	3.0612363	0.00809	0.431007	0.0003325	3090.125	290.0188
0.8794311	1.277643	3.0612315	0.006236	0.431005	0.0003325	4008.897	290.0198
0.8794312	1.277641	3.0612268	0.004382	0.431004	0.0003325	5705.195	290.0208
0.8794313	1.277639	3.061222	0.002528	0.431002	0.0003325	9889.982	290.0218
0.8794314	1.277637	3.0612173	0.000674	0.431001	0.0003325	37111.35	290.0227
0.8794315	1.277635	3.0612125	−0.00118	0.430999	0.0003325	21177.19	290.0237
0.8794316	1.277633	3.0612078	−0.00303	0.430998	0.0003325	8238.099	290.0247
0.8794317	1.277631	3.061203	−0.00489	0.430996	0.0003325	5113.68	290.0257
0.8794318	1.277629	3.0611983	−0.00674	0.430995	0.0003325	3707.54	290.0267
0.8794319	1.277627	3.0611935	−0.0086	0.430993	0.0003325	2907.928	290.0276
0.879432	1.277625	3.0611888	−0.01045	0.430992	0.0003325	2392.034	290.0286
0.8794321	1.277623	3.061184	−0.01231	0.430991	0.0003325	2031.607	290.0296
0.8794322	1.277621	3.0611793	−0.01416	0.430989	0.0003325	1765.573	290.0306
0.8794323	1.277619	3.0611745	−0.01601	0.430988	0.0003325	1561.145	290.0315
0.8794324	1.277617	3.0611698	−0.01787	0.430986	0.0003325	1399.144	290.0325
0.8794325	1.277615	3.061165	−0.01972	0.4309847	0.0003325	1267.604	290.0335
0.8794326	1.277613	3.0611603	−0.02158	0.4309832	0.0003325	1158.672	290.0345
0.8794327	1.277611	3.0611555	−0.02343	0.4309818	0.0003325	1066.98	290.0355
0.8794328	1.277609	3.0611508	−0.02528	0.4309803	0.0003325	988.7366	290.0364
0.8794329	1.277607	3.061146	−0.02714	0.4309789	0.0003325	921.1843	290.0374
0.879433	1.277605	3.0611413	−0.02899	0.4309774	0.0003325	862.2722	290.0384
0.8794331	1.277603	3.0611366	−0.03085	0.430976	0.0003325	810.4422	290.0394
0.8794332	1.277601	3.0611318	−0.0327	0.4309745	0.0003325	764.4898	290.0403
0.8794333	1.277599	3.0611271	−0.03456	0.4309731	0.0003325	723.4688	290.0413
0.8794334	1.277597	3.0611223	−0.03641	0.4309716	0.0003325	686.6258	290.0423
0.8794335	1.277595	3.0611176	−0.03826	0.4309702	0.0003325	653.3534	290.0433
0.8794336	1.277593	3.0611128	−0.04012	0.4309687	0.0003325	623.1566	290.0443
0.8794337	1.277591	3.0611081	−0.04197	0.4309673	0.0003325	595.6277	290.0452
0.8794338	1.277589	3.0611033	−0.04383	0.4309658	0.0003325	570.4281	290.0462
0.8794339	1.277587	3.0610986	−0.04568	0.4309643	0.0003325	547.2743	290.0472
0.879434	1.277585	3.0610938	−0.04754	0.4309629	0.0003324	525.9267	290.0482

References

1. Born, M.; Wolf, E. *Princiiples of Optics*; Cambridge University Press: Cambridge, UK, 1999; pp. 14–24.

2. Shelby, R.A.; Smith, D.R.; Shultz, S.; Nemat-Nasser, S.C. Microwave transmission through a two-dimensional, isotropic, left-handed metamaterial. *Appl. Phys. Lett.* **2001**, *78*, 489–491. [CrossRef]
3. Smith, D.R.; Padilla, W.J.; Vier, D.C.; Nemat-Nasser, S.C.; Schultz, S. Composite Medium with Simultaneously Negative Permeability and Permittivity. *Phys. Rev. Lett.* **2000**, *84*, 4184–4187. [CrossRef] [PubMed]
4. Group Velocity Dispersion. Available online: https://www.thorlabs.us/images/TabImages/AFS_prisms_GVD_G2-480.gif (accessed on 22 February 2018).
5. Third Order Dispersion. Available online: https://www.thorlabs.us/images/TabImages/AFS_prisms_TOD_G2-480.gif (accessed on 22 February 2018).
6. Smith, D.R.; Pendry, J.B.; Wiltshire, M.C.K. Metamaterials and negative refractive index. *Science* **2004**, *305*, 788–792. [CrossRef] [PubMed]
7. Engheta, R.; Ziolkowski, R.W. *Metamaterials, Physics and Engineering Explorations*; Wiley-IEEE: New York, NY, USA, 2006.
8. Shalaev, V.M. Optical negative-index metamaterials. *Nat. Photonics* **2007**, *1*, 41–48. [CrossRef]
9. Liu, Y.; Zhang, X. Metamaterials: A new frontier of science and technology. *Chem. Soc. Rev.* **2011**, *40*, 2494–2507. [CrossRef] [PubMed]
10. Soukoulis, C.M.; Wegener, M. Past achievements and future challenges in the development of three-dimensional photonic metamaterials. *Nat. Photonics* **2011**, *5*, 523–530. [CrossRef]
11. Zheludev, N.I.; Kivshar, Y.S. From metamaterials to metadevices. *Nat. Mater.* **2012**, *11*, 917–924. [CrossRef] [PubMed]
12. Zheludev, N.I.; Plum, E. Reconfigurable nanomechanical photonic metamaterials. *Nat. Nanotechnol.* **2016**, *11*, 16–22. [CrossRef] [PubMed]
13. Zheludev, N.I. Obtaining optical properties on demand. *Science* **2015**, *348*, 973–974. [CrossRef] [PubMed]
14. Dastmalchi, B.; Tassin, P.; Koschny, T.; Soukoulis, C.M. Strong group-velocity dispersion compensation with phase-engineered sheet metamaterials. *Phys. Rev. B* **2014**, *89*, 115123. [CrossRef]
15. Veselago, V.G. Electrodynamics of substances with simultaneously negative electrical and magnetic permeabilities. *Sov. Phys. Usp.* **1968**, *10*, 504–509. [CrossRef]
16. Pendry, J.B.; Holden, A.J.; Stewart, W.J.; Youngs, I. Extremely Low Frequency Plasmons in Metallic Mesostructures. *Phys. Rev. Lett.* **1996**, *76*, 4773–4776. [CrossRef] [PubMed]
17. Pendry, J.B.; Holden, A.J.; Robbins, D.J.; Stewart, W.J. Magnetism from conductors and enhanced nonlinear phenomena. *IEEE Trans Microw. Theory Tech.* **1999**, *47*, 2075–2084. [CrossRef]
18. Shelby, R.A.; Smith, D.R.; Schultz, S. Experimental verification of a negative index of refraction. *Science* **2011**, *292*, 77–79. [CrossRef] [PubMed]
19. Agrawal, G.P. *Nonlinear Fiber Optics*, 5th ed.; Academic Press: Cambridge, MA, USA, 2013.
20. Liu, Y.; Xue, Y.L.; Yu, C. Modulation instability induced by cross-phase modulation in negative index materials with higher-order nonlinearity. *Opt. Commun.* **2015**, *339*, 66–73. [CrossRef]
21. Shalaev, V.M.; Cai, W.; Chettiar, U.K.; Yuan, H.; Sarychev, A.K.; Drachev, V.P.; Kildishev, A.V. Nagative index of refraction in optical metamaterials. *Opt. Lett.* **2005**, *30*, 3356–3358. [CrossRef] [PubMed]
22. Wen, S.; Wang, Y.; Su, W.; Xiang, Y.; Fu, X.; Fan, D. Modulation instability in nonlinear negative-index material. *Phys. Rev. E* **2006**, *73*, 036617. [CrossRef] [PubMed]
23. Alù, A.; Salandrino, A. Negative effective permeability and left-handed materials at optical frequencies. *Opt. Express* **2006**, *14*, 1557–1567. [CrossRef] [PubMed]
24. YXue, L.; Liu, W.; Gu, Y.; Zhang, Y. Light storage in a cylindrical waveguide with metamaterials. *Opt. Laser Technol.* **2015**, *68*, 28–35.
25. Ordal, M.A.; Bell, R.J.; Alexander, R.W., Jr.; Long, L.L.; Querry, M.R. Optical properties of fourteen metals in the infrared and far infrared: Al, Co, Cu, Au, Fe, Pb, Mo, Ni, Pd, Pt, Ag, Ti, V, and W. *Appl. Opt.* **1985**, *24*, 4493–4499. [CrossRef] [PubMed]
26. Ordal, M.A.; Long, L.L.; Bell, R.J.; Bell, S.E.; Bell, R.R.; Alexander, R.W.; Ward, C.A. Optical properties of the metals Al, Co, Cu, Au, Fe, Pb, Ni, Pd, Pt, Ag, Ti, and W in the infrared and far infrared. *Appl. Opt.* **1983**, *22*, 1099–1119. [CrossRef] [PubMed]